

See discussions, stats, and author profiles for this publication at: <https://www.researchgate.net/publication/340970840>

# Investigation on the Electrochemical Behaviour and Deposition Mechanism of Neodymium in $\text{NdF}_3\text{-LiF-Nd}_2\text{O}_3$ Melt on Mo Electrode

Article in *Metals - Open Access Metallurgy Journal* · April 2020

DOI: 10.3390/met10050576

CITATIONS

0

READS

60

6 authors, including:



**Vesna S. Cvetković**  
University of Belgrade

37 PUBLICATIONS 85 CITATIONS

[SEE PROFILE](#)



**Dominic Feldhaus**  
RWTH Aachen University

3 PUBLICATIONS 1 CITATION

[SEE PROFILE](#)



**Nataša M. Vukićević**  
Scientific Institution Institute of Chemistry, Technology and Metallurgy Univerity ...

24 PUBLICATIONS 18 CITATIONS

[SEE PROFILE](#)



**Bernd Friedrich**  
RWTH Aachen University

654 PUBLICATIONS 2,357 CITATIONS

[SEE PROFILE](#)

Some of the authors of this publication are also working on these related projects:







Zone melting refining [View project](#)



European Training Network for Zero-waste Valorisation of Bauxite Residue (Red Mud) (REDMUD) MSCA-ETN project [View project](#)

## Article

# Investigation on the Electrochemical Behaviour and Deposition Mechanism of Neodymium in $\text{NdF}_3\text{--LiF--Nd}_2\text{O}_3$ Melt on Mo Electrode

Vesna S. Cvetković <sup>1,\*</sup> , Dominic Feldhaus <sup>2</sup>, Nataša M. Vukićević <sup>1</sup> , Tanja S. Barudžija <sup>3</sup> , Bernd Friedrich <sup>2</sup>  and Jovan N. Jovićević <sup>1</sup>

<sup>1</sup> Department of Electrochemistry, Institute of Chemistry, Technology and Metallurgy, National Institute, University of Belgrade, Njegoševa 12, 110000 Belgrade, Serbia; vukicevic@ihtm.bg.ac.rs (N.M.V.); jovicevic@ihtm.bg.ac.rs (J.N.J.)

<sup>2</sup> IME Process Metallurgy and Metal Recycling, Institute of RWTH Aachen University, Intzestrasse 3, 52056 Aachen, Germany; DFeldhaus@ime-aachen.de (D.F.); bfriedrich@ime-aachen.de (B.F.)

<sup>3</sup> Institute for Nuclear Sciences Vinča, University of Belgrade, P.O.Box 522, 11001 Belgrade, Serbia; tbarudzija@vin.bg.ac.rs

\* Correspondence: v.cvetkovic@ihtm.bg.ac.rs; Tel.: +381-11-3640-228

Received: 16 March 2020; Accepted: 25 April 2020; Published: 28 April 2020



**Abstract:** Neodymium was electrochemically deposited from  $\text{NdF}_3\text{--LiF--Nd}_2\text{O}_3$  molten salt electrolyte onto the Mo electrode at temperatures close to 1273 K. Cyclic voltammetry and chronoamperometry measurements were the applied electrochemical methods. Metallic neodymium is obtained by potentiostatic deposition. The optical microscopy and XRD were used to analyze the electrolyte, the working electrode surface, and the deposit on the electrode. It was established that Nd(III) ions were reduced to Nd metals in two steps:  $\text{Nd(III)} + \text{e}^- \rightarrow \text{Nd(II)}$  at potential  $\approx -0.55$  V vs. W and  $\text{Nd(II)} + 2\text{e}^- \rightarrow \text{Nd(0)}$  at  $\approx -0.83$  V vs. W. Both of these processes are reversible and under mass transfer control. Upon deposition under the regime of relatively small deposition overpotential of  $-0.10$  V to  $-0.20$  V, and after the electrolyte was cooled off, Nd metal was observed at the surface of the Mo electrode. CO and  $\text{CF}_4$  were gases registered as being evolved at the anode. CO and  $\text{CF}_4$  evolution were observed in quantities below 600 ppm and 10 ppm, respectively.

**Keywords:** neodymium electrodeposition; fluoride melts; cyclic voltammetry; gas emission

## 1. Introduction

Rare earth metals are increasing in importance, particularly in the production of permanent magnets, energy, high technology, and electronic devices [1–4]. Due to their rare occurrence in nature and the difficulties encountered in extracting and refining them, rare earth metals are expensive. Potential supply risks appear to be an additional important issue [3]. To meet long-term sustainable supply, efforts to improve recycling and recovery of product waste from magnets or electronic scraps and spent nuclear fuels are of great importance [4–6]. For example, rare earths, known as a neutron poisons, made up almost a quarter of the fission products in spent nuclear fuel [2]. Recycling of this waste can result in recovery of rare earth metals, including neodymium, a metal which constitutes roughly one third of rare earths [2]. Meanwhile, it was confirmed that electrolytic production and refining are promising techniques for achieving energy-efficient recovery of rare earth elements [3]. As a result, high-temperature rare earths molten salt electrolysis has become a subject of intensive research and development [3,7,8]. Characterization of electrochemical behaviour of rare earth metals in molten salts should provide a further guide for the next steps in development and optimization of the recycling industrial processes.

To recover neodymium as a pure metal on an inert cathode by electrowinning, it requires a suitable combination of neodymium salts and solvents to compose a melt which will serve as an appropriate electrolyte [9]. Commonly investigated salt combinations include chlorides, fluorides, and oxides of alkali and alkaline earth metals and neodymium [8,10,11]. The electrolytes made of molten chlorides are mainly composed of  $\text{NdCl}_3 + \text{LiCl} + \text{KCl}$  [1–3,7,11–16]. Fluoride electrolytes are considered more suitable because of their higher conductivity, lower hygroscopy, and higher current efficiency of the neodymium deposition compared to the chloride melts [17,18]. Most of the molten fluoride electrolytes for Nd electrowinning was found in the literature reference  $\text{LiF}$  ( $\text{NaF}$  or  $\text{KF}$ ) with  $\text{CaF}_2$  (or  $\text{BaF}_2$ ) [8,10,17–29].  $\text{NdF}_3$  and  $\text{Nd}_2\text{O}_3$  serve as sources of neodymium in such fluoride melts.

In both, chloride and fluoride electrolyte systems, a common observation is the low current efficiency of Nd electrodeposition. This is especially pronounced in the chloride electrolyte systems. Substantial efforts were made to investigate inadequate Nd deposition efficiency [3,18]. These considerations are particularly focused on the disproportionation reaction between the electrodeposited metal Nd and  $\text{Nd}^{3+}$  ions, which are permanently present in the melt, leading to  $\text{Nd}^{2+}$  ion production. The additional obstacle seems to be that the  $\text{Nd}^{2+}$  ion is chemically stable at temperatures lower than 810–840 K in a chloride system [7], and at temperatures around 1273 K in a fluoride system [18].

In the publications devoted to electrochemical behaviour of neodymium in the molten fluoride electrolyte, the data on the mechanism of neodymium(III) reduction are limited and contradictory. Observed yields of electrochemically deposited Nd are generally low due to side reactions [3,15,17,18].

The objective of this work is to acquire additional knowledge on the electrodeposition of Nd from molten fluoride electrolyte onto a molybdenum electrode. More specifically, to investigate the reaction mechanism of Nd deposition, which would favour more metal neodymium remaining on the electrode surface, better control of the process, greenhouse gas emission reduction during electrolysis, and better Nd deposition efficiency.

## 2. Materials and Methods

The stainless-steel cell, which was used for the electrochemical experiments, is shown in Figure 1. A graphite crucible was filled with electrolyte and placed in the cell. The electrolyte consisted of 87.5 wt.% neodymium fluoride ( $\text{NdF}_3$ , Treibacher, Althofen, Austria,  $\geq 99.9\%$ ) and 12.5 wt.% lithium fluoride ( $\text{LiF}$ , STREM Chemicals, Inc., Newburyport, MA, United States, 99.9%). This molar ratio of 47.5 mol%  $\text{NdF}_3$  and 52.5 mol%  $\text{LiF}$  proved to be the most suitable in terms of the melting temperature and viscosity of the electrolyte [22]. The preparation of these electrolyte components included drying for 24 h at 523 K before the two powders were premixed, fed into a high purity graphite crucible, then melted and homogenized in a vacuum induction furnace under an argon atmosphere of 1800 mbar at up to 1373 K. An additional chemical compound was added to the electrolyte, neodymium oxide ( $\text{Nd}_2\text{O}_3$ , Treibacher, Althofen, Austria, 99.8%), which was dried for 24 h at 393 K. In order to make this material more suitable for the feeding process (the addition into the electrolyte already in the cell), the dried powder was pressed, crushed, and sieved to achieve a powder particle size between 0.71 mm and 2 mm. All of the experiments were conducted with 2 wt.% of  $\text{Nd}_2\text{O}_3$  in the  $\text{NdF}_3$ – $\text{LiF}$  electrolyte in order to minimize sample to sample variation.

The working electrode (WE) was a molybdenum wire (Mo, 1 mm diameter, EWG, Weissach-Flacht, Germany, 99.95%), the reference electrode (RE) was a tungsten wire (W, 2 mm diameter, EWG, Weissach-Flacht, Germany, 99.9%), and the counter electrode was a glassy carbon rod (GC, 4 mm diameter, HTW SIGRADUR®G, Thierhaupten, Germany,  $>99.99\%$ ). All the reported potentials of WE in this work were measured relative to the tungsten RE in the melts used under given conditions.

All the electrodes were polished and, prior to each experiment, rinsed with deionized water and methanol, dried, and mounted into the cell. The immersion depth of the electrodes into the electrolyte was 1 cm.

The cell was placed into a resistance-heated furnace and heated up to 1433 K in order to reach the target temperature of 1323 K in the electrolyte. The temperature was measured by a thermocouple Type B via the Swagelok connection. The cell was supplied with a water-cooled lid with Swagelok connections, which assured that the electrodes can be inserted into the cell while it was still gas-tight (Figure 1). This was necessary to prevent the escape of harmful gases formed in the cell during the experiments.

During the experiments, argon flow (1.5 L/min) was introduced into the cell to flush the system and prevent the melt from having contact with air. The offgases formed were led into washing bottles filled with water and NaOH, before being treated by the exhaust system.

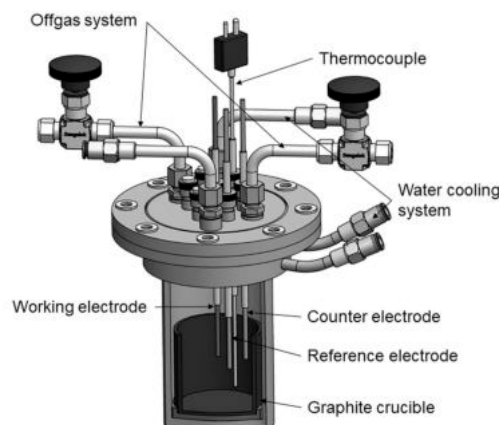


Figure 1. Experimental setup.

The electrochemical measurements were conducted by an IviumStat potentiostat (5 A and 10 V; Ivium Technologies, Eindhoven, The Netherlands).

The characterization of the cathodic behaviour was done using the electrochemical measuring methods, cyclic voltammetry and chronoamperometry.

The cyclic voltammograms were obtained on a molybdenum working electrode in a molten  $\text{NdF}_3\text{--LiF--Nd}_2\text{O}_3$  electrolyte, and started from potential  $E_I$ , usually 0.05 V more negative than the Mo open-circuit potential (measured against the tungsten reference electrode), changed to a final cathodic end potential,  $E_F$ , and back with various sweep rates.

In the second procedure, the same potential range was scanned with a sweep rate of  $100 \text{ mV}\cdot\text{s}^{-1}$ , but the scan was interrupted when the potential reached  $-0.80 \text{ V}$ ; and this potential was held for 5, 60, and 180 s before starting the return scan.

Potentiostatic electrodeposition onto molybdenum and tungsten electrodes in the molten  $\text{NdF}_3\text{--LiF--Nd}_2\text{O}_3$  electrolyte system was initiated 5 min after insertion of the working electrode into the melt, in order to allow thermal equilibrium. Neodymium was electrodeposited at a different constant overpotential at 1323 K. After the deposition, the working electrode was taken out of the melt, but kept inside the cell. The system was then cooled, and the electrode was taken out from the cell and kept under vacuum, awaiting further analysis. The morphology of the sample deposits were explored by optical microscope (Keyence; model VH-Z100R, Osaka, Osaka Prefecture, Japan). The deposit obtained on the working electrode and electrolyte collected near the working electrode at 1323 K were analysed by X-ray diffraction (XRD) with a Philips PW 1050 powder diffractometer (Philips, Delft, The Netherlands) at room temperature with Ni filtered  $\text{CuK}\alpha$  radiation ( $\lambda = 1.54178 \text{ \AA}$ ), scintillation detector within  $20\text{--}85^\circ$   $2\theta$  range in steps of  $0.05^\circ$ , and scanning time of 5 s per step, or by SmartLab®X-ray diffractometer (Rigaku Co., Tokyo, Japan) using  $\text{Cu K}\alpha$  radiation ( $\lambda = 1.542 \text{ \AA}$ ). The patterns were collected within a  $2\theta$  range of  $10\text{--}90^\circ$  at a scan rate of  $0.5^\circ/\text{min}$  with divergent slit of 0.5 mm, operated at 40 kV and 30 mA. The phases formed during the deposition were identified by comparison of the recorded diffraction peaks with the references from the Joint Committee on Powder

Diffraction Standards (JCPDS) database. During electrodeposition, off-gas measurements were done by Gasmet DX4000 Fourier transformation infrared spectrometer (FTIR, Ansyco, Karlsruhe, Germany).

### 3. Results and Discussion

Cyclic voltammograms were first recorded on a molybdenum working electrode in the electrolyte made of  $\text{NdF}_3$ –LiF molten salt mixture. Although the melt composition is very important for potential use in the extraction processes of neodymium, only little research has been focused on the structure of neodymium electrolytes, and only some qualitative results about the forms of complex ions have been published [28]. In the  $\text{NdF}_3$ –LiF molten salt mixture,  $\text{NdF}_3$  reacts with  $\text{F}^-$ , dissociated from molten LiF, to form Nd–F complex ions. Some authors assumed [28] that the main form of the Nd–F complex ion is  $[\text{NdF}_4]^-$ , others [17], after studying the structure of  $\text{NdF}_3$ –LiF melt by Raman spectrometry, recommended the existence of  $[\text{NdF}_6]^{3-}$ . The generally accepted viewpoint is that  $[\text{NdF}_6]^{3-}$ ,  $[\text{NdF}_4]^-$ , and  $\text{F}^-$  coexist in these melts [28,29]. In the temperature range of 1223–1323 K, the molar fraction of  $[\text{NdF}_6]^{3-}$ ,  $[\text{NdF}_4]^-$ , and  $\text{F}^-$  in all anions is expected to be 22 to 25 mol%, 25 mol%, and 50 to 52 mol%, respectively. It appears that  $[\text{NdF}_6]^{3-}$  is prone to decomposing into  $[\text{NdF}_4]^-$  and  $\text{F}^-$  with an increase in temperature [28].

The voltammograms obtained using various scan rates on the Mo electrode, from the  $\text{NdF}_3$ –LiF molten salt electrolyte, are presented in Figure 2. In the potential range between  $-0.05$  V and  $-0.90$  V, two cathodic current waves can be registered and attributed to the reduction of Nd ions: a broad cathodic wave at around  $-0.55$  V, and its anodic counterpart at  $\approx -0.35$  V; and a second cathodic peak starting at around  $-0.83$  V, and its anodic response at  $\approx -0.70$  V. These voltammograms suggest that the cathodic and anodic processes recorded reflect the deposition and dissolution of the Nd metal on the cathode [18,20,25].

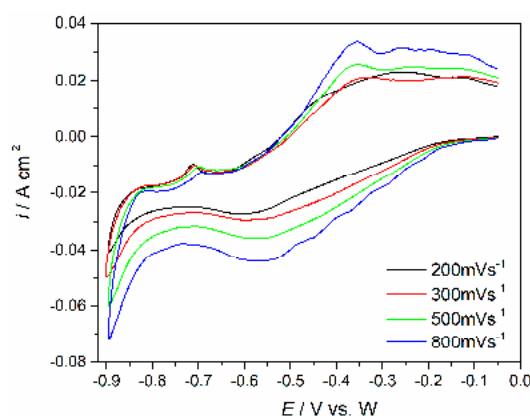


**Figure 2.** Cyclic voltammograms recorded with different sweep rates on Mo electrode in  $\text{NdF}_3$ –LiF molten salt electrolyte, at 1323 K; the potential range used:  $E_i = -0.05$  V to  $E_f = -0.90$  V.

The voltammograms recorded using the same working electrode (Mo) in the same  $\text{NdF}_3$ –LiF electrolyte but with added  $\text{Nd}_2\text{O}_3$  (2 wt.%), are shown in Figure 3. In the electrolyte with the  $\text{Nd}_2\text{O}_3$  added, the cathodic and anodic current waves are more clearly defined, and the maximum peak current densities recorded are several times higher (Figure 3) than in the electrolyte without  $\text{Nd}_2\text{O}_3$  present (Figure 2). In the presence of  $\text{Nd}_2\text{O}_3$  and at potentials negative to  $-0.10$  V, (Figure 3a,b), two distinct regions of cathodic/anodic activities can be observed. The peak pair at  $\approx -0.59$  V (I) and  $\approx -0.39$  V (I'), and the second peak pair at  $\approx -0.76$  V (II) and  $\approx -0.59$  V (II') indicate two consecutive reversible redox reactions. When the applied potential was shifted more cathodic to  $-1.00$  V, a new pair of current waves was observed (III/III').

The cathodic peak (I) at  $\approx -0.59$  V (Figure 3a–c) should reflect the reduction of Nd(III) to Nd(II) and the reduction peak (II) at  $\approx -0.76$  V should record reduction of Nd(II) into metal Nd. The corresponding anodic signals in the reverse scan, (II') at  $\approx -0.59$  V should relate to the dissolution of metal Nd, and

the anodic peak at  $\approx -0.37$  V to the oxidation of Nd(II) into Nd(III). The cathodic peak (III) and the corresponding anodic peak (III') in the reverse scan (Figure 3a) were not subjects of this investigation. The same conclusions based on very similar voltammograms obtained from identical or very similar fluoride electrolytes support the said deliberations [18,20,25].

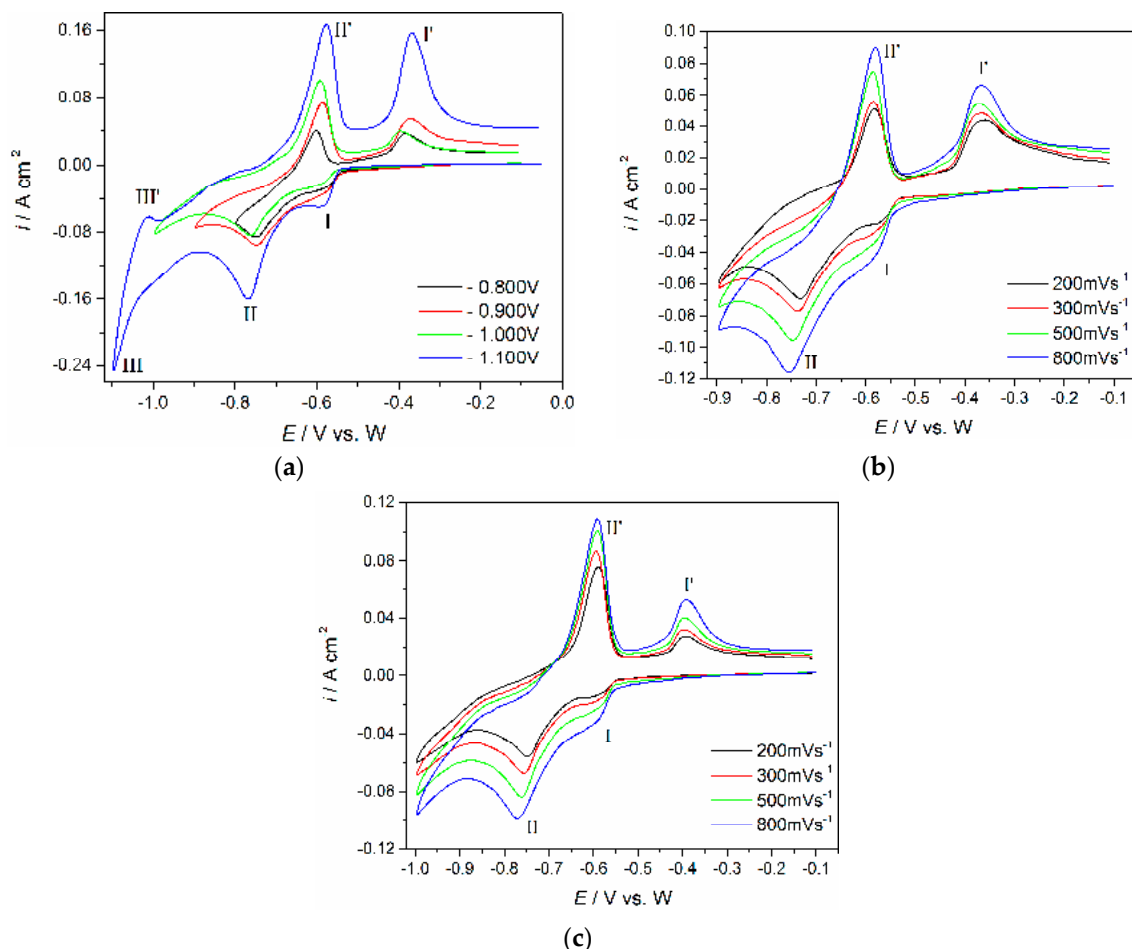


**Figure 3.** Cyclic voltammograms recorded on Mo working electrode in  $\text{NdF}_3\text{--LiF} + (2 \text{ wt.}\%) \text{Nd}_2\text{O}_3$  molten salt electrolyte, at 1323 K: (a)  $v = 500 \text{ mV}\cdot\text{s}^{-1}$ , potential range was from  $-0.10$  V to a different cathodic end potential; (b) potential range from  $-0.10$  V to  $-0.90$  V scanned with different sweep rates; (c) potential range from  $-0.10$  V to  $-1.00$  V scanned with different sweep rates.

The dissolution of  $\text{Nd}_2\text{O}_3$  in molten fluoride ( $\text{LiF--NdF}_3$ ) is a diffusion-controlled process which can be accelerated if the temperature and  $\text{NdF}_3$  concentration in the melt are increased [30]. However,  $\text{Nd}_2\text{O}_3$  has very limited solubility in fluoride melts ( $\text{LiF--CaF}_2\text{--NdF}_3$ ,  $\text{LiF--KF--NdF}_3$ , etc.). Its concentration in the melts is 1–5 mass% at 1373 K and much smaller than the concentrations of LiF,  $\text{CaF}_2$ , or  $\text{NdF}_3$  [31]. Nevertheless, when added to the fluoride melt,  $\text{Nd}_2\text{O}_3$  dissolves in the presence of LiF and  $\text{NdF}_3$  and forms oxyfluorides,  $\text{NdOF}$  or  $[\text{NdOF}_5]^{4-}$  [28,29,31,32]:



Given that the electrolyte has an excess of  $\text{F}^-$ ,  $[\text{NdF}_6]^{3-}$  and  $[\text{NdOF}_5]^{4-}$  coexist. Which of the two species will be predominantly involved in the neodymium deposition reaction should depend on the neodymium oxyfluoride ions/neodymium fluoride ions molar ratio [17,29], electrode potential, and current density applied [24]. The source of Nd metals at high current densities, high voltage

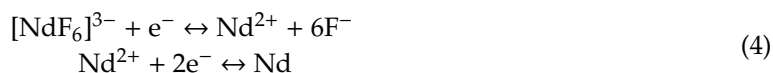
electrolysis, and low  $[\text{NdOF}_5]^{4-}/[\text{NdF}_6]^{3-}$  molar ratio is  $[\text{NdF}_6]^{3-}$ . At low current densities, low voltage electrolysis, and high  $[\text{NdOF}_5]^{4-}/[\text{NdF}_6]^{3-}$  molar ratio, it is  $[\text{NdOF}_5]^{4-}$  [29]. The electroreduction of neodymium from neodymium fluorides or neodymium oxyfluorides on inert electrodes (W, Mo, glassy carbon) is a process that is still not defined. In fact, the electroreduction of Nd(III) to Nd(0) from fluoride electrolytes was explained in the literature as a one-step process [6,17,19,21,26,27,29,32] or a two-step process [18,20,25]:

(A) from neodymium fluorides:

(a) in one step

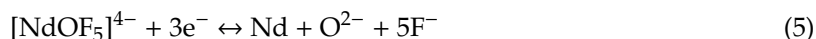


(b) in two steps

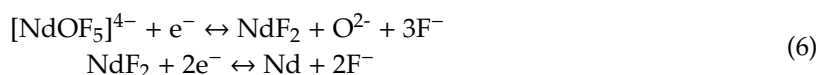


(B) from neodymium oxyfluoride, a very complicated process, but can be described as:

(a) in one step



(b) in two steps



To follow up on the processes indicated in neodymium deposition/dissolution in the  $\text{NdF}_3\text{--LiF--Nd}_2\text{O}_3$  melt on Mo revealed by cyclic voltammograms, cyclic voltammetry using different holding times at negative potential end of the cycle was applied (Figure 4).

The cathodic end potential of the molybdenum working electrode was held at  $-0.80$  V for 5, 60, and 180 s, before letting the potential return to positive values (Figure 4). According to the results presented in Figure 3, the chosen cathodic end potential should represent the neodymium deposition overpotential of  $\approx -0.15$  V. This assumption was very well supported by the increase of maximum peak currents and the charge encompassed by the anodic current waves (II' and I'), with increased deposition time. Increased charge within anodic current wave II', which reflects reaction  $\text{Nd} - 2e^- \rightarrow \text{Nd(II)}$  with increased deposition time indicates more metal neodymium being dissolved. This confirms, that with prolonged times of the deposition under the applied overpotential ( $\approx -0.15$  V), more metal Nd was previously deposited. The enlarged quantity of the Nd(II) complexed ions provided by the neodymium (anodic peaks II') increases the quantity of the Nd(III) ions formed in the consecutive oxidation  $\text{Nd(II)} \rightarrow \text{Nd(III)}$  reaction (anodic peak I'). This is reflected as increased peak currents and increased charges encompassed by the anodic current wave (I'), in Figure 4.

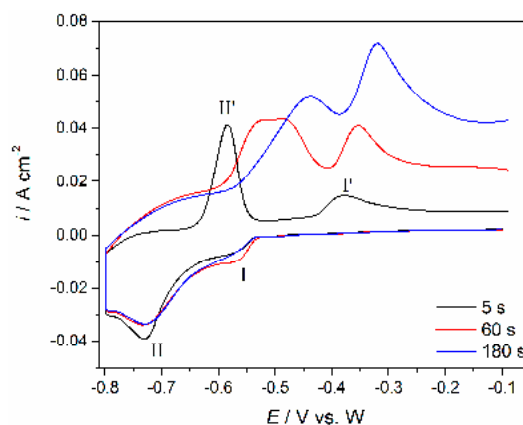


**Figure 4.** Voltammograms obtained from Mo working electrode in  $\text{NdF}_3\text{--LiF--Nd}_2\text{O}_3$  melt with different “holding times” ( $\tau = 5, 60$  and  $180$  s) at negative end potential of the cycle ( $-0.80$  V); sweep rate  $100 \text{ mV}\cdot\text{s}^{-1}$ ,  $T = 1323$  K.



This confirmed the assumption, that Nd metal can be electrodeposited on molybdenum electrode, in a two-step reduction process of Nd(III)  $\rightarrow$  Nd(II) and Nd(II) into Nd(0) [18,20,25]. This was reflected in our measurements at  $\approx -0.57$  V and  $\approx -0.73$  V, respectively.

The results recorded by the applied electrochemical techniques are in accordance with the literature that states that the electrochemical reduction of Nd(III) ions on molybdenum electrode in molten  $\text{NdF}_3\text{-LiF-Nd}_2\text{O}_3$  electrolyte is a two-step process [18,20,25]. The possibility that the two redox reactions (namely: Nd(III)  $\leftrightarrow$  Nd(II) and Nd(II)  $\leftrightarrow$  Nd(0)) reflected by the current peaks, I/I' and II/II', shown in the voltammograms in Figure 3 are reversible and diffusion controlled, was investigated in the analysis (Figure 5), which included the relationship between peak currents recorded and the square root of the scanning rates applied [33]. Voltammograms shown in Figure 3b,c exhibit responses to the scan rates increased from  $200 \text{ mV}\cdot\text{s}^{-1}$  to  $800 \text{ mV}\cdot\text{s}^{-1}$ , within the potential range from  $-0.10$  V to  $-0.80$  V and  $-1.00$  V. Maximum current densities of the cathodic ((I) and (II)) and anodic peaks ((I') and (II')) increased, but their peak potential differential was relatively small. The plots derived from Figure 3c using the cathodic (I) and its counterpart anodic peak (I') current densities versus the square root of the scan rates applied, appeared to be linear but did not pass through the origin (Figure 5a). This should indicate that the redox process Nd(III)  $\leftrightarrow$  Nd(II) is under mixed control: by the diffusion of the complexed Nd ions and the rate of their charge transfer step, which includes complicated disbanding and formation of the ligand complexes [18]. In addition, the plots derived from Figure 3c, representing the peak currents for the peak (II) versus the square root of the scan rates applied, proved to be linear as well and it also did not pass through the origin (see Figure 5b). This implies that the redox process of Nd(II)  $\leftrightarrow$  Nd(0) on the molybdenum cathode is also controlled by diffusion of complexed Nd ions in the molten  $\text{NdF}_3\text{-LiF-Nd}_2\text{O}_3$  electrolyte, and the rate of the charge transfer step is additionally complicated by the dismantling of fluoride and oxyfluoride complex formations [18,20,25].

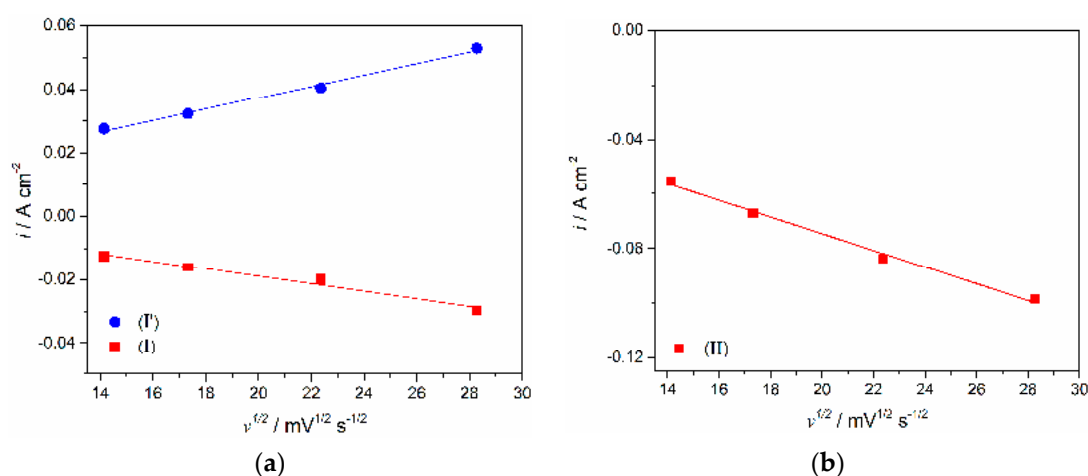


**Figure 5.** Cathodic and anodic peak currents density vs. the square root of the scan rates derived from Figure 3c; (a) of peaks (I/I') and (b) of peak (II).

The data recorded in Figure 3 offers the possibility of establishing the number of exchanged electrons in the reversible reactions represented by the peak pairs, I/I' and II/II' [18,34]. Figure 6 provides a graphical presentation of the function  $\log i_p = f(E_p)$ , obtained by correlating the values of the peak current logarithms with the peak potentials recorded for different potential scan rates in Figure 3. The logarithms of the current density values characteristic for the cathodic (I) peak potentials recorded for four different scan rates are plotted in Figure 6a. Figure 6b shows the results of the same procedure applied to the anodic peak (II'). The dissolution peak was used to additionally support the claim for the reversibility of the Nd(II)  $\leftrightarrow$  Nd(0) reaction. According to the deliberations already mentioned [18,34], the slope  $K$  of the functions  $\log i_p = f(E_p)$  graphically presented in Figure 6 is defined as:

$$K = \alpha z F / 2.3RT \quad (7)$$



where  $\alpha = 0.5$ ,  $F$  is the Faraday constant,  $R$  is the gas constant,  $T$  is the absolute temperature, and  $z$  is the number of exchanged electrons. The slope for the cathodic peaks I (Figure 6a) was 2.12, and the electron transfer number is 1.1 which is close to 1, implying electrochemical reduction of  $\text{Nd(III)} \rightarrow \text{Nd(II)}$ . According to the data in Figure 6b, the slope was 3.3 and the electron transfer number is 1.73 which is close to 2, implying electrochemical oxidation of  $\text{Nd(0)} \rightarrow \text{Nd(II)}$ .

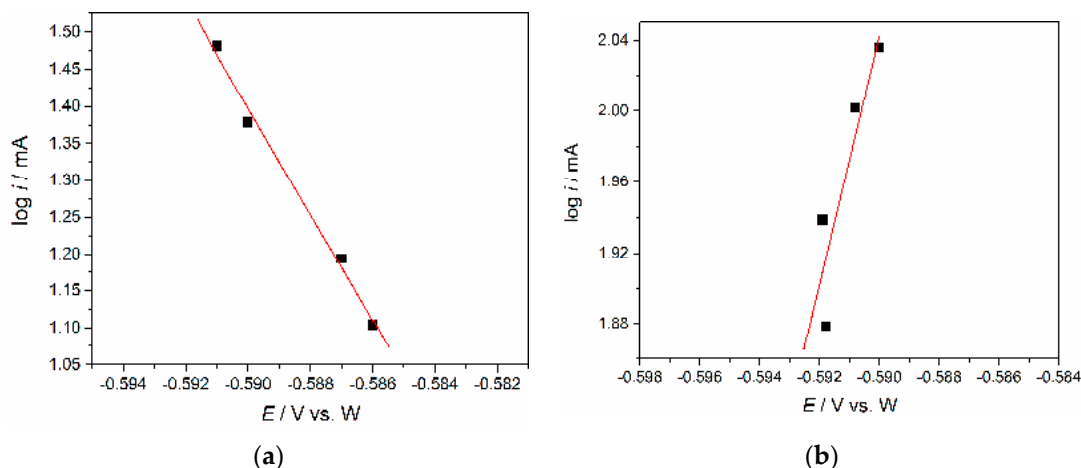
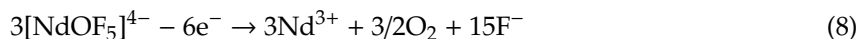


**Figure 6.** Logarithm of the peak current density vs. peak potential from the voltammograms in Figure 3c: (a) for the cathodic current wave (I); (b) for the anodic current wave (II').

These results should confirm that in the system investigated, neodymium  $\text{Nd(III)}$  ions are electrochemically reduced to  $\text{Nd(0)}$  in two reversible steps:  $\text{Nd(III)} + e^- \leftrightarrow \text{Nd(II)}$  and  $\text{Nd(II)} + 2e^- \leftrightarrow \text{Nd(0)}$ , both of which are complicated by  $\text{Nd}$  ion mass transfer and construction, as well as decomposition of their ligand shells.

Meanwhile, in this system, there are a number of possible reactions that can take part on the anode:



When a GC electrode is used, the produced oxygen species can subsequently react with carbon producing  $\text{CO}$  and  $\text{CO}_2$ . With  $\text{F}^-$  present,  $\text{CF}_4$  and  $\text{C}_2\text{F}_6$  gases could also be evolved from a GC anode [22,35]. Serious efforts by the workers in this field are devoted to restricting the gas evolution to only oxygen, if possible. Anodic gases observed during the neodymium depositions performed, were recorded and their evolved amounts were measured, see Figure 7.

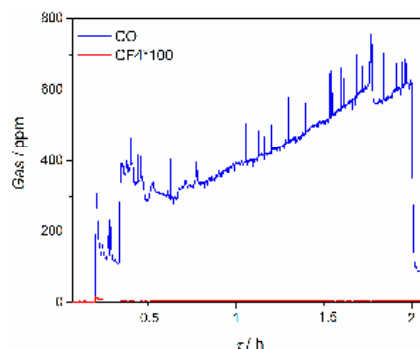
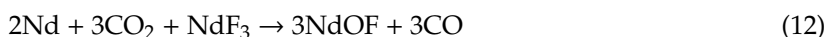


**Figure 7.** Gases evolved on the GC anode during potentiostatic Nd deposition at  $-0.80 \text{ V}$  on Mo electrode from the electrolyte used.

Carbon monoxide was observed in variable quantities, but always below 600 ppm. After a certain period of deposition time, the quantity of CO became substantially smaller, which might be attributed to the partial passivation of the anode active sites with oxygen containing ions [22]. CF<sub>4</sub> was recorded in very small quantities, well below 10 ppm. These findings might be attributed to a low deposition overpotential used at the cathode side of the cell, which was matched with an equally small anodic overpotential, which was obviously more negative than the fluorine evolution potential.

It should be noted that there are several other oxidation side reactions that may take place in the electrolyte used in this work [31]:



It can be assumed that the abundance of F<sup>−</sup> in the vicinity of Nd<sup>3+</sup>, produced at the anode from oxidation of [NdOF<sub>5</sub>]<sup>4−</sup>, leads to the formation of the [NdF<sub>6</sub>]<sup>3−</sup> species. Thus, the neodymium fluoride, which is consumed at the cathode through Equation (1), is eventually regenerated at the anode. Therefore, the electrodeposition of Nd proceeds at the expense of the neodymium oxide, provided that the electrolysis voltage is controlled so that no oxidation of fluoride ions is allowed. The fluoridising agent is constantly regenerated in-situ, which enables the continuous conversion of the added neodymium oxide into the corresponding fluoride [32].

When a constant potential of −0.90 V was applied for 5400 s on the Mo working electrode in the electrolyte made of NdF<sub>3</sub>–LiF, the XRD analysis of the electrolyte layer closely attached to the electrode, exhibited the presence of NdF<sub>3</sub>, NdF<sub>2</sub>, and LiF, which was very similar to the results obtained from the analysis of the NdF<sub>3</sub>–LiF–Nd<sub>2</sub>O<sub>3</sub> electrolyte layer formed on the same electrode under similar conditions (−0.80 V), shown in Figure 8.

Considering that the applied potential was 100 mV more negative than the peak potential value of the current wave (II) in Figure 3, which is suspected to reflect the Nd(II) into Nd(0) process, the XRD analysis of the electrolyte layer adhering to the electrode and electrode surface itself should have shown the presence of Nd. However, XRD analysis of the Mo electrode with a thin film of solidified electrolyte did not show Nd being present (Figure 8). The XRD spectrum for the sample in Figure 8a, obtained after deposition at −0.80 V for 7200 s, in the molten NdF<sub>3</sub>–LiF–Nd<sub>2</sub>O<sub>3</sub> electrolyte system, is exhibited in Figure 8b. The diffraction peaks recorded at 2θ = 24.71°, 25.31°, 28.23°, 35.67°, 41.15°, 44.61°, 45.71°, 50.67°, 51.66°, 53.63°, 56.47°, 58.38°, 65.80°, 69.78°, 70.63°, 72.53°, 75.55°, and 76.34° are characteristic of hexagonal NdF<sub>3</sub> [JCPDS No. 01-078-1859]. The diffraction peaks identified at 2θ = 38.76°, 65.63°, and 78.91° are attributed to face centered cubic LiF [01-072-1538]. The diffraction peaks at 2θ = 27.25°, 31.47°, 45.13°, 53.51°, and 56.02° should reflect face centered cubic NdF<sub>2</sub> [JCPDS No. 00-033-0934]. However, the peaks with slight variations in 2θ values at 27.1°, 31.44°, 45.03°, 53.39°, and 55.99° could indicate the presence of NdOF, but such a diffractogram should show some additional peaks characteristic of NdOF also [JCPDS No. 00-050-0635]. Those additional peaks were not recorded and we selected NdF<sub>2</sub> as the recognised phase. Also, the presence of NdF<sub>2</sub> in the deposit close to the working electrode surface should reflect the disproportionate reaction between Nd<sup>3+</sup> and Nd metal deposited. When the solidified electrolyte seen in Figure 8a was removed from the electrode and the Mo electrode surface in Figure 9a and analyzed again by XRD, metal neodymium was recognized on the electrode surface in addition to Mo, NdF<sub>2</sub>, and NdF<sub>3</sub> (Figure 9b). The diffraction peaks identified at 2θ values of 29.18°, 32.06°, 36.40°, 46.13°, 49.85°, 63.29°, and 75° are characteristic of hexagonal Nd [JCPDF No. 03-065-3424].

Similar results were obtained in XRD analysis of the W working electrode exposed to the similar potentiostatic regime in the same electrolyte (Figure 10). The deposition was done in the same time period and at the potential of −0.78 V.

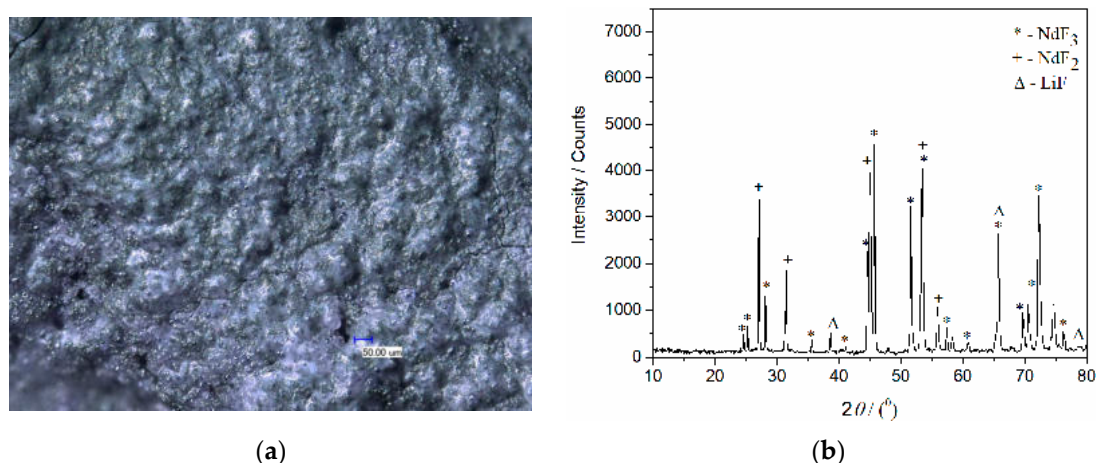


**Figure 8.** (a) Optical image of the Mo WE with closely attached electrolyte after deposition at  $-0.80$  V for 7200 s, in molten  $\text{NdF}_3\text{-LiF-Nd}_2\text{O}_3$  electrolyte system, at 1323 K (200×); (b) XRD spectra of the electrolyte layer on the Mo electrode from Figure 8a.

Neodymium metal was registered in a substantial quantity, and the peaks with  $2\theta$  values of  $30.28^\circ$ ,  $41.83^\circ$ ,  $48.06^\circ$ ,  $54.93^\circ$ ,  $59.45^\circ$ ,  $60.52^\circ$ ,  $62.98^\circ$ ,  $67.05^\circ$ , and  $77.30^\circ$ , characteristic of metal Nd were recognized [JCPDF No. 03-065-3424].

References to chronopotentiometric electrodeposition found in literature describe getting neodymium metal in the form of drops found in the electrolyte after cooling off the system [6,20,21,24,26,31].

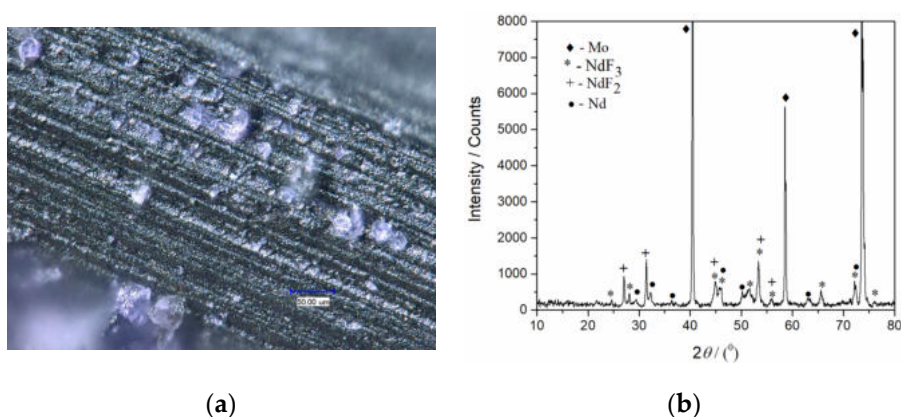


**Figure 9.** (a) Optical image of the Mo working electrode after deposition at  $-0.80$  V for 7200 s in molten  $\text{NdF}_3\text{-LiF-Nd}_2\text{O}_3$  electrolyte system, at 1323 K (the solidified electrolyte was removed from the electrode surface, magnification 600×); (b) XRD spectra of the Mo working electrode from Figure 9a.

There is only one example of Nd metal being identified on the inert cathode (Mo and W) surface by a deposition similar to the potentiostatic deposition from a fluoride molten salt electrolyte of the same composition in the literature available [18]. There are, however, papers showing XRD results of neodymium being deposited from fluoride melts on the working electrode, but only in the form of alloys [6,29,31].

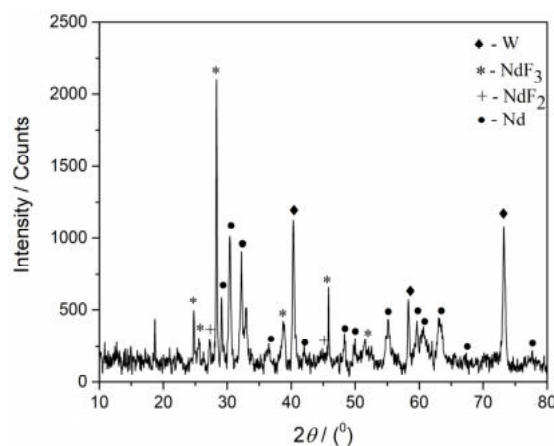


**Figure 10.** XRD spectra of the W working electrode surface after deposition at  $-0.78$  V for 7200 s, in molten  $\text{NdF}_3\text{-LiF-Nd}_2\text{O}_3$  electrolyte system, at 1323 K (the solidified electrolyte was removed from the electrode and the W electrode was analyzed).

There is also one identifying Nd metal on Mo substrate obtained by galvanostatic electrodeposition [26]. In the present literature, one can find many more references to the galvanostatic electrodeposition of Nd from fluoride melts than about potentiostatic electrodeposition [6,20,21,24,31]. All of the above suggests that the amount of the deposited Nd metal that remains on the electrode surface is very small, and therefore it is difficult to be recognized by XRD methods when even a very thin layer of the solidified electrolyte is covering the electrode. Usually, the metal, which is in a liquid state due to the working temperature, is forced by gravitation to leave the electrode surface in the shape of drops and finds the way through the electrolyte to the bottom of the cell.

The coexistence of Nd(II) and Nd(III) in the electrolyte in the presence of metal Nd leads to a spontaneous reaction of disproportionation (comproportionation) [18]:



This disproportionation reaction is unavoidable as soon as the first amounts of Nd metal are electrodeposited on a working electrode. Figure 11 exhibits a micrograph of the surface of a thin layer of the electrolyte adherent to the Mo cathode, obtained after 3600 s of potentiostatic deposition. The XRD analysis revealed that the black layer, which was closely attached to the Mo WE, consists entirely of  $\text{NdF}_2$  and  $\text{NdF}_3$  in accordance with Equation (14). In order to downgrade the influence of the disproportionation on the Nd electrodeposition yield efficiency, metal neodymium is sometimes added to the electrolyte to replace the freshly deposited Nd in the reaction Equation (14) [20].

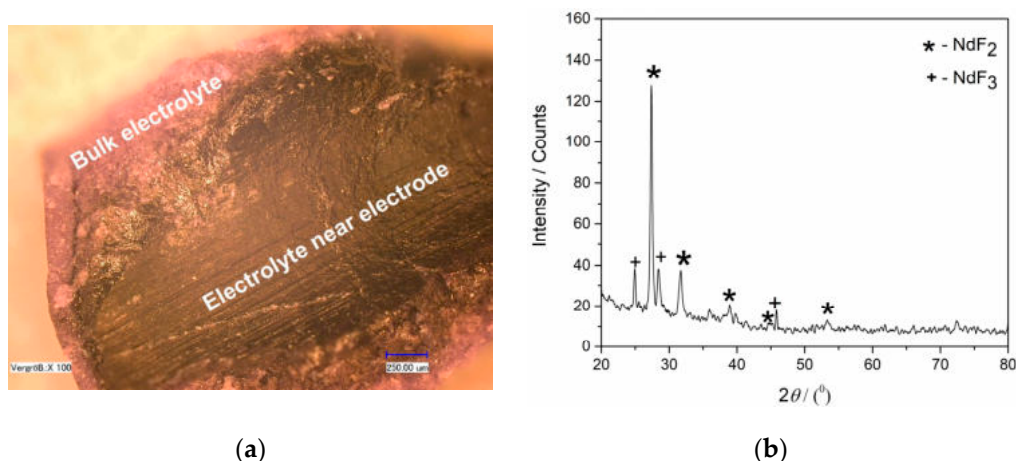


**Figure 11.** (a) Optical micrographs of the electrolyte peeled of the Mo electrode after 3600 s deposition at  $-0.90$  V in molten  $\text{NdF}_3\text{-LiF-Nd}_2\text{O}_3$  electrolyte, at 1323 K; (b) XRD spectra of the electrolyte surface which was next to the electrode surface.

#### 4. Conclusions

Electrochemical reduction processes of neodymium ions in  $\text{LiF-NdF}_3$  and  $\text{LiF-NdF}_3\text{-Nd}_2\text{O}_3$  melts were characterized by cyclic voltammetry measurements, and potentiostatic deposition was done on a Mo electrode. The electrolyte, the working electrode, and the deposit on the electrode were analyzed by optical microscopy and XRD.

In this study, a novel method was adopted, in which relatively small neodymium deposition overpotential is used to deposit more metallic Nd on the cathode and preventing fluorocarbon evolution at the anode. Very small quantities of  $\text{CO/CO}_2$  (less than 600 ppm), and negligible amounts of  $\text{CF}_4$  were recorded to have been evolved. Thus, at the anode in-situ regenerated fluoridizing agent  $\text{F}^-$  is at disposal to continuously convert the added  $\text{Nd}_2\text{O}_3$  into corresponding fluorides.

Metallic neodymium is obtained by potentiostatic deposition performed under relatively small deposition overpotentials ( $-100$  to  $-200$  mV). Neodymium was deposited by reduction of  $\text{Nd(III)}$  complexed ions in two steps:  $\text{Nd(III)} + \text{e}^- \rightarrow \text{Nd(II)}$  and  $\text{Nd(II)} + 2\text{e}^- \rightarrow \text{Nd(0)}$ . The first step takes place at the potential of  $\approx -0.55$  V, and the second at  $\approx -0.83$  V. Both processes are greatly controlled by mass transfer of the ions, but also by the rates of making and breaking of their complexes with  $\text{F}^-$  and  $\text{OF}^{3-}$  ligands.

Applied potentiostatic conditions allowed the metallic neodymium to remain at the cathode after cooling off the system. No Nd metal drops were recognized in the cooled electrolyte. Absence of the metal drops in the electrolyte should reduce the Nd metal surface that is otherwise available for disproportionation (comproportionation) reactions with  $\text{Nd(II)}$  and thus might increase current efficiency of Nd electrodeposition.

**Author Contributions:** V.S.C. was in charge of the methodology and participated in the manuscript preparation; D.F. performed most of the experiments, N.M.V. investigated and participated in the manuscript preparation; T.S.B. performed XRD data curation; B.F. and J.N.J. helped with the corrections of the manuscript and supervised; B.F. from RWTH Aachen University provided funding for publication. All authors discussed the results and commented on the manuscript. All authors have read and agreed to the published version of the manuscript.

**Funding:** Part of this research was supported by the funds of the bilateral research project (ID: 451-03-01971/2018-09/4), supported by the Ministry of Education, Science and Technological Development of the Republic of Serbia and German Academic Exchange Service (DAAD).

**Acknowledgments:** Vesna S. Cvetković and Nataša M. Vukićević acknowledge the financial support for the investigation received from the Ministry of Education, Science and Technological Development of the Republic of Serbia.

**Conflicts of Interest:** The authors declare no conflicts of interest.



## References

1. Hua, Z.; Liu, H.; Wang, J.; He, J.; Xiao, S.; Xiao, Y.; Yang, Y. Electrochemical Behavior of Neodymium and Formation of Mg-Nd Alloys in Molten Chlorides. *ACS Sustain. Chem. Eng.* **2017**, *5*, 8089–8096. [\[CrossRef\]](#)
2. Tang, H.; Pesic, B. Electrochemistry and the mechanisms of nucleation and growth of neodymium during electroreduction from LiCl-KCl eutectic salts on Mo substrate. *J. Nucl. Mater.* **2015**, *458*, 37–44. [\[CrossRef\]](#)
3. Shen, D.; Akolkar, R. Electrodeposition of Neodymium from NdCl<sub>3</sub>-Containing Eutectic LiCl-KCl Melts Investigated Using Voltammetry and Diffusion-Reaction Modeling. *J. Electrochem. Soc.* **2017**, *164*, H5292–H5298. [\[CrossRef\]](#)
4. Castrillejo, Y.; Fernández, P.; Medina, J.; Vega, M.; Barrado, E. Chemical and electrochemical extraction of ytterbium from molten chlorides in pyrochemical processes. *Electroanalysis* **2011**, *23*, 222–236. [\[CrossRef\]](#)
5. Fukasawa, K.; Uehara, A.; Nagai, T.; Fujii, T.; Yamana, H. Electrochemical and spectrophotometric study on neodymium ions in molten alkali chloride mixtures. *J. Alloys Compd.* **2011**, *509*, 5112–5118. [\[CrossRef\]](#)
6. Nohira, T.; Kobayashi, S.; Kondo, K.; Yasuda, K.; Hagiwara, R.; Oishi, T.; Konishi, H. Electrochemical Formation of RE-Ni (RE = Pr, Nd, Dy) Alloys in Molten Halides. *ECS Trans.* **2013**, *50*, 473–482. [\[CrossRef\]](#)
7. Novoselova, A.; Smolenski, V. Electrochemical behavior of neodymium compounds in molten chlorides. *Electrochim. Acta* **2013**, *87*, 657–662. [\[CrossRef\]](#)
8. Yang, Y.; Lan, C.; Guo, L.; An, Z.; Zhao, Z.; Li, B. Recovery of rare-earth element from rare-earth permanent magnet waste by electro-refining in molten fluorides. *Sep. Purif. Technol.* **2020**, *233*, 116030. [\[CrossRef\]](#)
9. Zhang, Q.; Hua, Y.; Xu, C.; Li, Y.; Li, J.; Dong, P. Non-haloaluminate ionic liquids for low-temperature electrodeposition of rare-earth metals—A review. *J. Rare Earths* **2015**, *33*, 1017–1025. [\[CrossRef\]](#)
10. Taxil, P.; Chamelot, P.; Massot, L.; Hamel, C. Electrodeposition of alloys or compounds in molten salts and applications. *J. Min. Metall. Sect. B Metall.* **2003**, *39*, 177–200. [\[CrossRef\]](#)
11. Diaz, L.; Chamelot, P.; Gibilaro, M.; Massot, L.; Serp, J. Electrochemical Behavior of Neodymium in Molten Chloride Salts. In *Minerals, Metals and Materials Series*; Kim, H., Ed.; Springer: New York, NY, USA, 2017; Volume Part F3, pp. 77–86. ISBN 9783319510842.
12. Castrillejo, Y.; Bermejo, M.R.; Barrado, E.; Martínez, A.M.; Díaz Arocas, P. Solubilization of rare earth oxides in the eutectic LiCl-KCl mixture at 450 °C and in the equimolar CaCl<sub>2</sub>-NaCl melt at 550 °C. *J. Electroanal. Chem.* **2003**, *545*, 141–157. [\[CrossRef\]](#)
13. Uehara, A.; Fukasawa, K.; Nagai, T.; Fujii, T.; Yamana, H. Separation of Nd metal by using disproportionation reaction of Nd(II) in molten chlorides. *J. Nucl. Mater.* **2011**, *414*, 336–339. [\[CrossRef\]](#)
14. Liu, K.; Liu, Y.-L.; Chai, Z.-F.; Shi, W.-Q. Evaluation of the Electroextractions of Ce and Nd from LiCl-KCl Molten Salt Using Liquid Ga Electrode. *J. Electrochem. Soc.* **2017**, *164*, D169–D178. [\[CrossRef\]](#)
15. Öhl, J. Challenges in electrolysis of neodymium in chloride melts at 500 °C. *J. Appl. Electrochem.* **2018**, *48*, 765–772. [\[CrossRef\]](#)
16. Xu, H.; Zhang, M.; Yan, Y.; Sun, X.; Zheng, Y.; Qiu, M.; Liu, L. Extraction of neodymium from other fission products by co-reduction of Sn and Nd. *Appl. Organomet. Chem.* **2019**, *33*, 1–10. [\[CrossRef\]](#)
17. Stefanidaki, E.; Hasiotis, C.; Kontoyannis, C. Electrodeposition of neodymium from LiF-NdF<sub>3</sub>-Nd<sub>2</sub>O<sub>3</sub> melts. *Electrochim. Acta* **2001**, *46*, 2665–2670. [\[CrossRef\]](#)
18. Huang, C.; Liu, X.; Gao, Y.; Liu, S.; Li, B. Cathodic processes of neodymium(III) in LiF-NdF<sub>3</sub>-Nd<sub>2</sub>O<sub>3</sub> melts. *Faraday Discuss.* **2016**, *190*, 339–349. [\[CrossRef\]](#)
19. Lee, G.G.; Jo, S.K.; Lee, C.K.; Ryu, H.Y.; Lee, J.H. Study on electrolysis for neodymium metal production. *TMS Annu. Meet.* **2015**, 15-19-Marc, 249–252.
20. Liu, X.; Huang, C.; Li, B. The effects of NdF<sub>2</sub> on current efficiency of Nd extraction from NdF<sub>3</sub>-LiF-Nd<sub>2</sub>O<sub>3</sub> melts. *Mater. Trans.* **2017**, *58*, 395–399. [\[CrossRef\]](#)
21. Chen, Z.; She, C.; Zheng, H.; Huang, W.; Zhu, T.; Jiang, F.; Gong, Y.; Li, Q. Electrochemical deposition of neodymium in LiF-CaF<sub>2</sub> from Nd<sub>2</sub>O<sub>3</sub> assisted by AlF<sub>3</sub>. *Electrochim. Acta* **2018**, *261*, 289–295. [\[CrossRef\]](#)
22. Milicevic, K.; Feldhaus, D.; Friedrich, B. Conditions and mechanisms of gas emissions from didymium electrolysis and its process control. In *Minerals, Metals and Materials Series*; Martin, O., Ed.; Springer: New York, NY, USA, 2018; Volume Part F4, pp. 1435–1441. ISBN 9783319722832.
23. Abbasalizadeh, A.; Teng, L.; Sridhar, S.; Seetharaman, S. Neodymium extraction using salt extraction process. *Trans. Inst. Min. Metall. Sect. C Miner. Process. Extr. Metall.* **2015**, *124*, 191–198. [\[CrossRef\]](#)

24. Kaneko, A.; Yamamoto, Y.; Okada, C. Electrochemistry of rare earth in molten salts. *J. Alloys Compd.* **1993**, *193*, 44–46. [\[CrossRef\]](#)
25. Shiguan, C.; Xiaoyong, Y.; Zhongxing, Y.; Qingtao, L. Cathodic Process of Nd and its Dissolution Behaviour in Molten Fluoride. *Rare Met.* **1994**, *13*, 46–49.
26. Hamel, C.; Chamelot, P.; Taxil, P. Neodymium(III) cathodic processes in molten fluorides. *Electrochim. Acta* **2004**, *49*, 4467–4476. [\[CrossRef\]](#)
27. Gibilaro, M.; Massot, L.; Chamelot, P.; Taxil, P. Study of neodymium extraction in molten fluorides by electrochemical co-reduction with aluminium. *J. Nucl. Mater.* **2008**, *382*, 39–45. [\[CrossRef\]](#)
28. Hu, X.; Wang, Z.; Gao, B.; Shi, Z.; Liu, F.; Cao, X. Density and ionic structure of NdF<sub>3</sub>–LiF melts. *J. Rare Earths* **2010**, *28*, 587–590. [\[CrossRef\]](#)
29. Thudum, R.; Srivastava, A.; Nandi, S.; Nagaraj, A.; Shekhar, R. Molten salt electrolysis of neodymium: Electrolyte selection and deposition mechanism. *Trans. Inst. Min. Metall. Sect. C Miner. Process. Extr. Metall.* **2010**, *119*, 88–92. [\[CrossRef\]](#)
30. Guo, X.; Sun, Z.; Sietsma, J.; Blanpain, B.; Guo, M.; Yang, Y. Quantitative Study on Dissolution Behavior of Nd<sub>2</sub>O<sub>3</sub> in Fluoride Melts. *Ind. Eng. Chem. Res.* **2018**, *57*, 1380–1388. [\[CrossRef\]](#)
31. Ciumag, M.; Gibilaro, M.; Massot, L.; Laucournet, R.; Chamelot, P. Neodymium electrowinning into copper-neodymium alloys by mixed oxide reduction in molten fluoride media. *J. Fluor. Chem.* **2016**, *184*, 1–7. [\[CrossRef\]](#)
32. Abbasalizadeh, A.; Seetharaman, S.; Venkatesan, P.; Sietsma, J.; Yang, Y. Use of iron reactive anode in electrowinning of neodymium from neodymium oxide. *Electrochim. Acta* **2019**, *310*, 146–152. [\[CrossRef\]](#)
33. Greef, R.; Peat, R.; Peter, L.M.; Pletcher, D.; Robinson, J. *Instrumental Methods in Electrochemistry*, 1st ed.; Kemp, T.J., Ed.; Ellis Horwood Limited: Chichester, UK, 1985; ISBN 0-85312-875-8.
34. Raoof, J.-B.; Omrani, A.; Ojani, R.; Monfared, F. Poly(N-methylaniline)/nickel modified carbon paste electrode as an efficient and cheap electrode for electrocatalytic oxidation of formaldehyde in alkaline medium. *J. Electroanal. Chem.* **2009**, *633*, 153–158. [\[CrossRef\]](#)
35. Vogel, H.; Flerus, B.; Stoffner, F.; Friedrich, B. Reducing Greenhouse Gas Emission from the Neodymium Oxide Electrolysis. Part I: Analysis of the Anodic Gas Formation. *J. Sustain. Metall.* **2017**, *3*, 99–107. [\[CrossRef\]](#)



© 2020 by the authors. Licensee MDPI, Basel, Switzerland. This article is an open access article distributed under the terms and conditions of the Creative Commons Attribution (CC BY) license (<http://creativecommons.org/licenses/by/4.0/>).